Equilibrium Unfolding of Dimeric Desulfoferrodoxin Involves a Monomeric Intermediate: Iron Cofactors Dissociate after Polypeptide Unfolding†

David Apiyo,‡ Kathryn Jones,§ Jesse Guidry,‡ and Pernilla Wittung-Stafshede*,‡,§

Chemistry Department and Molecular and Cellular Biology Graduate Program, Tulane University, New Orleans, Louisiana 70118

Received November 17, 2000; Revised Manuscript Received February 20, 2001

ABSTRACT: Here we report the conformational stability of homodimeric desulfoferrodoxin (dfx) from *Desulfovibrio desulfuricans* (ATCC 27774). The dimer is formed by two dfx monomers linked through β-strand interactions in two domains; in addition, each monomer contains two different iron centers: one Fe−(S-Cys)$_4$ center and one Fe−[S-Cys+(N-His)$_4$] center. The dissociation constant for dfx was determined to be 1 μM (ΔG = 34 kJ/mol of dimer) from the concentration dependence of aromatic residue emission. Upon addition of the chemical denaturant guanidine hydrochloride (GuHCl) to dfx, a reversible fluorescence change occurred at 2−3 M GuHCl. This transition was dependent upon protein concentration, in accord with a dimer to monomer reaction [$\Delta G(H_2O)$ = 46 kJ/mol of dimer]. The secondary structure did not disappear, according to far-UV circular dichroism (CD), until 6 M GuHCl was added; this transition was reversible (for incubation times of <1 h) and independent of dfx concentration [$\Delta G(H_2O)$ = 50 kJ/mol of monomer]. Thus, dfx equilibrium unfolding is at least three-state, involving a monomeric intermediate with native-like secondary structure. Only after complete polypeptide unfolding (and incubation times of >1 h) did the iron centers dissociate, as monitored by disappearance of ligand-to-metal charge transfer absorption, fluorescence of an iron indicator, and reactivity of cysteines to Ellman's reagent. Iron dissociation took place over several hours and resulted in an irreversibly denatured dfx. It appears as if the presence of the iron centers, the amino acid composition, and, to a lesser extent, the dimeric structure are factors that aid in facilitating dfx's unusually high thermodynamic stability for a mesophilic protein.

Previous work on protein folding has focused on small, single-domain proteins that fold rapidly and avoid aggregation. However, many proteins in the cell are large with multiple folding domains and/or subunits. Most likely, these large proteins do not follow all of the folding principles established for smaller proteins, and probably have more complex folding rules. Most proteins more than 100 residues long have been shown to fold via intermediate states. The folding of multimeric proteins involves not only the intramolecular interactions as a polypeptide chain associates with itself (monomer folding) but also the intermolecular interactions as it associates with other monomers (subunit assembly). How the amino acid sequence controls subunit−subunit interactions, and what additional stability is conferred by these intermolecular interactions, can only be addressed by characterization of oligomeric proteins. Unfolding pathways for oligomeric proteins have been shown to vary significantly. For example, tetrameric peanut agglutinin first dissociates to folded monomers and then the monomers unfold (*1*), whereas tetrameric SecB and dimeric dihydrofolate reductase convert to unfolded monomers without populating intermediate states (*2*, *3*). In the case of the tetrameric lactose repressor, the denatured state remains tetrameric due to very strong interface interactions (*4*). Moreover, dimeric class μ glutathione transferases unfold through monomeric intermediates (*5*), whereas unfolding of the SecA dimer proceeds through a dimeric intermediate (*6*). In the case of the heptameric chaperonin protein 10, unfolding in high concentrations of GuHCl[1] leads to a monomeric unfolded state whereas urea-induced unfolding instead favors an unfolded state in which the subunits remain assembled (*7*).

Another determinant that may affect the folding mechanism and the equilibrium stability of a protein is the presence of cofactors. More than 20% of all proteins in the cell coordinate cofactors in their native states to attain specific functions. It has been shown for proteins coordinating inorganic cofactors that the folded proteins are significantly stabilized by the cofactor (*8*−*11*). For example, *Escherichia coli* cytochrome b_{562} is at least 14 kJ/mol more stable toward unfolding when the oxidized heme is present, as compared to when in its apo form (*8*). When the heme is reduced, the stability of holocytochrome b_{562} increases further (*12*). In the case of the copper-binding protein azurin from *Pseudomonas aeruginosa*, the holo form is stabilized by almost 20 kJ/mol, as compared to the stability of the apoprotein, against

† The Louisiana Board of Regents [LEQSF(1999-02)-RD-A-39], the donors of the American Chemical Society Petroleum Research Fund, the National Science Foundation (Grant MCB-0075902), and the Keck Foundation (instrumentation) are acknowledged for financial support.

* Corresponding author. Phone: (504) 862-8943. Fax: (504) 865-5596. E-mail: pernilla@tulane.edu.

‡ Chemistry Department.

§ Molecular and Cellular Biology Graduate Program.

[1] Abbreviations: GuHCl, guanidine hydrochloride; CD, circular dichroism; dfx, desulfoferrodoxin.

10.1021/bi002653y CCC: $20.00 © 2001 American Chemical Society
Published on Web 03/28/2001

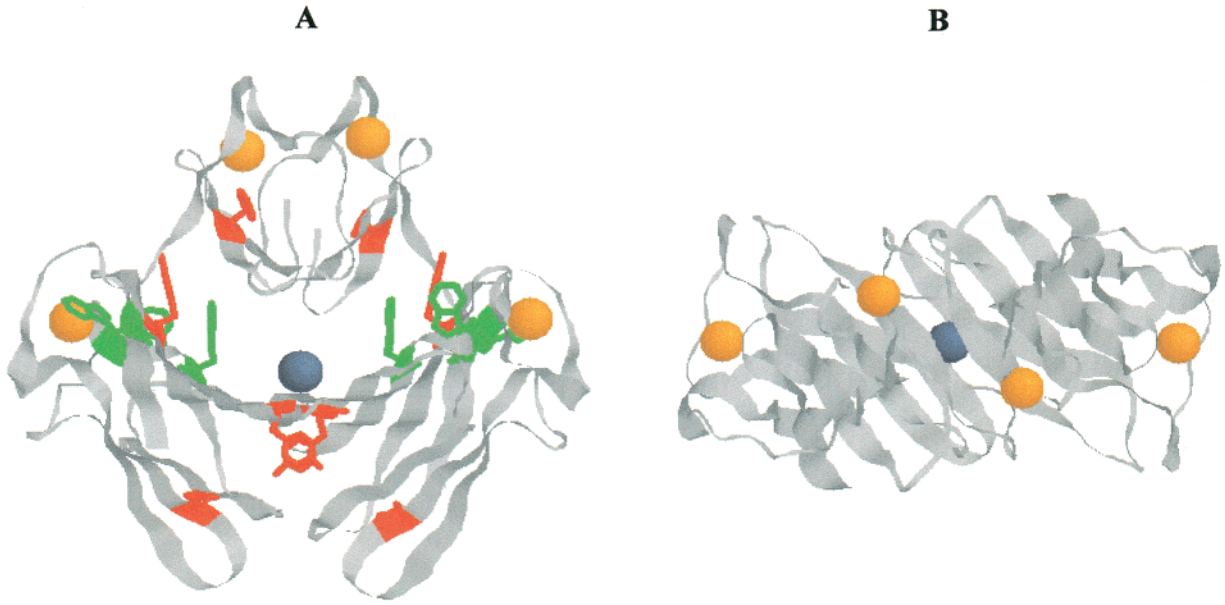

FIGURE 1: Ribbon diagram of the dfx dimer (PDB entry 1dfx). The calcium (dark gray), situated on the interface between the monomers, and the irons (yellow), one each in domain I and domain II of each monomer, are shown as space-filling diagrams. (A) Orientation of the dimer with the 2-fold crystallographic axis along the plane of the figure. Domain I is at the top and domain II at the bottom. Tryptophan (green) and tyrosine (red) residues are shown in stick representations. (B) Dimer viewed along the 2-fold axis.

GuHCl-induced unfolding (*9*). In contrast, the organic flavin mononucleotide cofactor (FMN) was shown to have no effect on *Desulfovibrio desulfuricans* flavodoxin equilibrium stability (*13*).

In addition to modulating polypeptide stability, cofactor coordination may induce local structure in unfolded proteins. Such structural restrictions in the unfolded ensemble of protein molecules may dramatically decrease the entropy of the unfolded state as well as limit the conformational search for the native state (*14*, *15*). Recent experimental findings emphasize the significance of cofactor binding to unfolded proteins in vitro (*8*, *16*), even when no covalent bonds are present between the cofactor and the polypeptide. Coordination of the hemes in cytochrome b_{562} and myoglobin to the corresponding unfolded polypeptides have been observed (*8*, *12*, *17*), and in the case of *P. aeruginosa* azurin and the *Thermus thermophilus* Cu_A domain (*9*, *18*, *19*), the copper ions stay bound to the unfolded polypeptides. FMN was found to remain associated with unfolded *D. desulfuricans* flavodoxin, albeit its binding site on the polypeptide is not yet established (*13*). Moreover, it was reported that for the high-potential iron−sulfur protein (HiPIP) from *Chromatium vinosum*, the polypeptide unfolded before the Fe_4S_4 cluster was degraded (*20*), and ferredoxin from the thermophilic archaeon *Acidianus ambivalens* was found to form new, possibly linear three-iron sulfur clusters upon polypeptide unfolding that subsequently decomposed (*21*). In the case of cytochrome *c* maturation in vivo, it is believed that heme is enzymatically inserted when the polypeptide is still unfolded; only after heme insertion is folding of the protein possible (*22*).

To probe the interplay between folding and assembly in an oligomeric protein, we have used dimeric desulfoferrodoxin (dfx) from *D. desulfuricans* (ATCC 27774) as our model (*23*−*25*). Since each dfx monomer contains two iron centers, we also addressed the involvement of these cofactors in the folding and assembly reaction. Dfx plays a role in the electron transfer chain of sulfate-reducing bacteria, although its precise functional activity is still unknown. Dfx has been found in several bacterial strains, including *Desulfovibrio vulgaris*, *D. desulfuricans*, *Methanobacterium thermoautotropicum*, and the human pathogen that causes syphilis, *Treponema pallidum* (*25*−*28*). The X-ray crystal structure of *D. desulfuricans* dfx was recently determined (*29*). The protein is a homodimer (2 × 14 kDa) with predominantly β-sheet structures that can be described in terms of two domains, each with two crystallographically equivalent nonheme mononuclear iron centers (Figure 1). Domain I (N-terminal part, about 4 kDa per monomer) is similar to desulforedoxin with distorted rubredoxin-type Fe−$(S\text{-}Cys)_4$ centers (center I), in which the iron ligands are Cys-9, Cys-12, Cys-28, and Cys-29. Domain II (C-terminal part, ∼10 kDa per monomer) has distinct iron centers (center II) with square pyramidal coordination of four histidine nitrogens as the equatorial ligands and one cysteine sulfur as the axial ligand (dfx residues His-48, His-68, His-74, His-118, and Cys-115). Three β-sheets extend from one dfx monomer to another, strongly supporting the assumption of dfx as a functional dimer [as also suggested by analytical gel filtration (*30*)]. In the dimer, domain I has two almost parallel β-sheets forming an incomplete β-barrel and domain II adopts an antiparallel β-sheet that extends through the molecule and one smaller β-sheet in each monomer that do not interact in the dimer. The iron atoms are found close to the molecular surface and are well exposed to the solvent. The monomer−monomer interface in the dfx dimer consists of two hydrophobic regions, with many aromatic residues; between these regions is a polar core of side chains in which, in the crystal structure, a calcium ion was found (Figure 1) (*29*). Also, the interface between the two domains in each monomer accommodates many aromatic residues; in particular, the three tryptophans located in domain II are near both monomer−monomer and domain−domain areas. Although dfx can exist in three redox states [fully oxidized (gray),

semireduced (pink), and fully reduced], our studies are confined to the aerobically stable semireduced state in which the iron in center I is oxidized and that in center II is reduced.

Here we report that equilibrium unfolding of dfx proceeds through a *monomeric* intermediate that has altered fluorescence but native-like secondary structure. The iron atoms do not dissociate until *after* incubation of the unfolded polypeptide. As long as the metals remain coordinated to the protein, the unfolding is reversible. Dfx is highly resistant to thermally induced and solvent-induced denaturation [$\Delta G(H_2O) = 145$ kJ/mol of dimer at 20 °C]. These properties are compared to those for other oligomeric proteins as well as discussed in the context of the dimer−interface interactions, the presence of iron centers, and the dfx amino acid composition, which is reminiscent of that of thermophilic proteins.

MATERIALS AND METHODS

Preparation of Dfx. Expression and purification of dfx has been described previously (*23*−*25*). Protein concentrations (in monomer units) were determined from an ϵ_{410} of 4980 M^{-1} cm^{-1}.

Spectroscopic Methods. Absorption spectra were measured on a Cary 50 spectrophotometer (1 cm cell). For far-UV circular dichroism (CD) measurements, an OLIS spectropolarimeter (1 cm cell for 1−5 μM dfx; 1 mm cell for >5 μM dfx) was used. For CD measurements, the sample compartment was purged with nitrogen gas to avoid absorption by O_2. Fluorescence spectra (1 cm cell, excitation at 280 or 290 nm) were collected on a Varian Eclipse fluorometer. All experiments (except thermal denaturation) were performed at 20 °C.

Denaturation Reactions. Chemical denaturant GuHCl (Sigma Chemicals) was of highest purity. The buffer in all denaturation and renaturation reactions was 5 mM sodium phosphate (pH 7.0). Denaturation was monitored by far-UV CD (200−260 nm), by fluorescence (290−400 nm), and by optical absorption (250−800 nm) at various protein concentrations (see Results and figure legends). Stock solutions of GuHCl (in different amounts) were mixed with dfx solutions to give constant, fixed final protein concentrations. Acquired data were analyzed as described below. Thermal denaturation of dfx was studied by monitoring the far-UV CD spectrum (200−250 nm) upon slowly increasing the temperature. The temperature was increased in steps of 5 °C (from 15 to 90 °C) and then decreased in one step back to 20 °C; 5 min of equilibration time was allowed at each temperature.

Analysis of Fluorescence-Monitored Denaturation. Since GuHCl-induced denaturation monitored by fluorescence was found to be protein concentration-dependent, each such transition was analyzed using the following mechanism (F, folded; I, intermediate), an apparent two-state reaction coupled to dissociation:

$$F_{dimer} \leftrightarrow 2I_{monomer} \quad (1)$$

The equilibrium constant, K_{F-I}, and the free energy change, ΔG_{F-I}, for reaction 1 are defined as

$$K_{F-I} = [F_{dimer}]/[I_{monomer}]^2 \quad (2)$$

$$\Delta G_{F-I} = -RT \ln K_{F-I} \quad (3)$$

Table 1: Thermodynamic Parameters for GuHCl-Induced Denaturation of Dfx, at Various Protein Concentrations, Monitored by Fluorescence (emission maximum) and Far-UV CD (secondary structure)

	fluorescence[a]		far-UV CD[b]	
[dfx] (μM)	$[GuHCl]_{1/2}$ (M)	$\Delta G_{F-I}(H_2O)$ (kJ/mol)	$[GuHCl]_{1/2}$ (M)	$\Delta G_{I-U}(H_2O)$ (kJ/mol)
0.2	1.7	—[c]	—[c]	—[c]
1.0	2.2	44.3 ± 2	5.2	51.4 ± 3
5.0[d]	2.3	47.5 ± 2	4.9	47.1 ± 3
20.0	2.9	45.8 ± 2	5.1	50.1 ± 3
		av. 45.9	av. 5.1	av. 49.5

[a] Analyzed in terms of a dimer to monomer transition; ΔG is per mole of dimer. [b] Analyzed in terms of a two-state (monomer to monomer) transition; ΔG is per mole of monomer. [c] Not determined due to weak signals. [d] For this dfx concentration, visible absorption was also recorded during GuHCl titration. The absorption from dfx's iron center I disappears with a transition midpoint occurring at 5.0 ± 0.1 M GuHCl; thus, it overlaps with the CD-monitored transition.

where $[F_{dimer}]$ is the concentration of folded dimers (in molar) and $[I_{monomer}]$ is the concentration of intermediate monomers (in molar) at each GuHCl concentration. Standard concentrations of 1 M of all reactants are introduced; R is the gas constant, and T is the absolute temperature. The use of a protein concentration of 1 M as the standard state is commonly used for concentration-dependent protein unfolding reactions (*2*−*4*, *31*). The free energy change can be expressed as a function of denaturant (here, GuHCl) concentration:

$$\Delta G_{F-I} = \Delta G_{F-I}(H_2O) - m[GuHCl] \quad (4)$$

In this equation, m describes the sensitivity of the transition to GuHCl and is thought to reflect the extent of hydrophobic surface exposure upon unfolding. $\Delta G_{F-I}(H_2O)$ is the free energy of the change in aqueous solution (in this case per mole of dimer). The free energy changes as functions of GuHCl concentration were fitted (in KaleidaGraph, Synergy Software) to eq 4. Values for $\Delta G_{F-I}(H_2O)$ at various dfx concentrations are listed in Table 1. The midpoints of the transitions were derived by inspection of the unfolding curves. Uncertainties for ΔG_{F-I} values were obtained by repeating the experiments.

Analysis of Far-UV CD-Monitored Denaturation. GuHCl-induced denaturation monitored by far-UV CD (monitoring signals at 210 and 230 nm gave identical results) occurred at higher denaturant concentrations than the fluorescence-monitored changes and was independent of dfx concentration. Therefore, each CD-monitored transition was analyzed using a two-state model without a dissociation step, assuming the presence of monomer only ($f_I + f_U = 1$). f_I and f_U represent the fraction of total protein in the intermediate (folded according to CD) and denatured conformations, respectively. The equilibrium constant, K_{I-U}, and the free energy change, ΔG_{I-U}, at each point in the reactions were calculated from eqs 3 and 5:

$$K_{I-U} = f_U/(1 - f_U) = f_U/f_I \quad (5)$$

Direct fits (in KaleidaGraph) to the experimental denaturation curves were performed using the following equation, derived from eqs 3−5:

$$Y_{obs} = [Y_U - Y_I(\exp\{[\Delta G_{I-U}(H_2O) - m[GuHCl]]/RT\})]/[1 + (\exp\{[\Delta G_{I-U}(H_2O) - m[GuHCl]]/RT\})] \quad (6)$$

Y_{obs}, Y_U, and Y_I are the observed CD signal, denatured protein baseline intensity, and intermediate protein baseline intensity, respectively. From the fits, values for $\Delta G_{I-U}(H_2O)$ were determined for each transition (Table 1). The midpoints of the CD transitions were calculated as $\Delta G_{I-U}(H_2O)/m$. Reported uncertainties for ΔG_{I-U} values were obtained from the goodness of the fits.

Ellman's Assay for Free Sulfurs. Investigation of the presence of free sulfhydryl groups in unfolded dfx was performed using Ellman's assay. In short, dfx samples in the presence of various GuHCl concentrations were first incubated for 5 min followed by visible absorption recordings. (Thiosulfo)benzoate (NTSB, 3 mM) was added to the samples in the presence and absence of 1 mM EDTA (pH 7.3) and the mixture incubated for an additional 5 min. Free sulfurs can react in a 1:1 ratio with NTSB to form the yellow 2-nitro-5-thiobenzoate (NTB). By using the extinction coefficient ($\epsilon_{412} = 14\,150\ M^{-1}\ cm^{-1}$) for NTB, the number of free sulfurs in each protein sample was in this way quantified. Control experiments with all components present except protein were also performed.

Iron Dissociation Probed by Phen Green. The fluorescent indicator for iron Phen Green (P-6801) was purchased from Molecular Probes. Phen Green emission is significantly quenched upon iron coordination. Emission (peak at 520−525 nm) was monitored, upon excitation at 492 nm, for samples of dfx (5 μM) in the presence of 100 μM Phen Green and variable amounts of GuHCl (0−6 M), incubated for 2 h. In control experiments, titrating $Fe(III)Cl_3$ into 100 μM Phen Green yielded a rough reference curve of quenching efficiency versus Fe(III) concentration under our conditions. The *Molecular Probes Handbook* reports that Phen Green quenching is ~1.5 times more efficient for Fe(II) than for Fe(III) binding.

RESULTS

Dfx Dimer−Monomer Dissociation Constant. The crystal structure and SDS−PAGE and gel filtration experiments suggest that dfx exists as a dimer in solution (*29*, *30*), although a monomeric state was proposed initially (*25*). Each dfx monomer contains four tyrosine (Y7, Y59, Y88, and Y114) and three tryptophan (W75, W87, and W121) residues mostly placed on, or near, the monomer−monomer interface (*29*). At low dfx concentrations, the emission per monomer (excitation at 280 nm, emission centered around 335 nm) is smaller than at higher dfx concentrations, presumably due to solvation of the aromatic residues (and emission quenching) upon dimer dissociation. Using this change in fluorescence, we determined the equilibrium constant for disassembly of the dfx dimer (Figure 2). Our measurements indicate a midpoint of dissociation (and thus the value for K_{diss}) at 1 ± 0.2 μM (monomer concentration), which equals a free energy of 34 ± 1 kJ/mol of dfx dimer. The presence of a high concentration (10 mM) of calcium ions or metal chelator EDTA in the buffer (data not shown) did not alter K_{diss}, suggesting that the calcium ion found on the dimer interface in the crystal structure does not affect the dimer−monomer equilibrium.

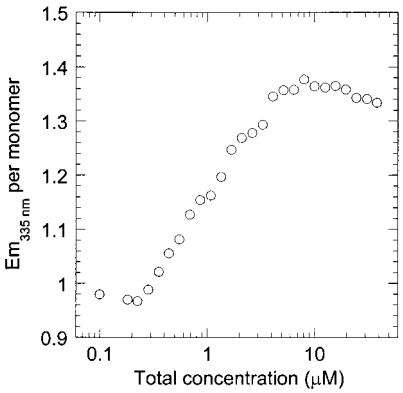

FIGURE 2: Relative fluorescence at 335 nm (upon excitation at 280 nm) per monomer for various total dfx concentrations. The transition midpoint occurs at 1 ± 0.2 μM dfx monomer. K_{diss} was estimated to be $1.0 \times 10^6\ M^{-1}$ using the equation $K_{diss} = [dimer]/[monomer]^2 = ([dfx]/4)/([dfx]/2)^2$ (eq 7), in which [dfx] = 1 μM, i.e., the total monomer concentration at the transition midpoint.

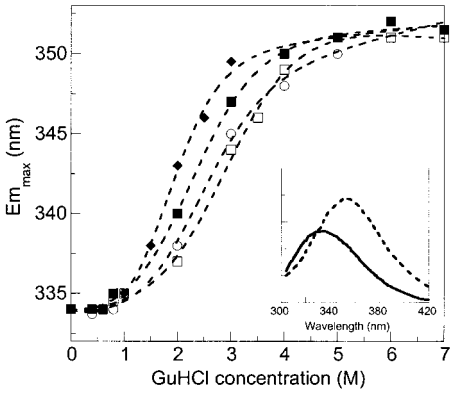

FIGURE 3: GuHCl-induced transitions in emission maxima placement for various total dfx concentrations [(◆) 0.2, (■) 1, (○) 5, and (□) 20 μM]. The inset shows the emission from native (—) and intermediate dfx (- - -) (see the text for an explanation).

GuHCl-Induced Denaturation of Dfx Monitored by Fluorescence. Upon addition of GuHCl to dfx at protein concentrations around or above the K_{diss} (0.2−20 μM monomer concentration), we observe a change in the emission maximum toward higher wavelengths. In buffer, the dfx emission is centered around 335 ± 1 nm, whereas at ≥4 M GuHCl, it appears around 352 ± 2 nm (Figure 3, inset). The GuHCl-induced transitions monitored by emission maximum change are dependent upon dfx concentration: the higher the protein concentration, the more GuHCl is required to induce a change in emission maxima (Figure 3 and Table 1). For example, the transition midpoints occur at 2.9 M GuHCl for 20 μM dfx but at 1.7 M GuHCl for 0.2 μM protein. This result indicates that the emission change probes an alteration in the oligomeric state of dfx: the higher the dfx concentration, the more resistant the protein is toward the denaturant. Sample excitation at 280 or 290 nm did not change the emission profiles, suggesting that the three tryptophans (and not the tyrosines) contribute most of the emission. The free energy change for this process analyzed in terms of a dimer to monomer reaction, when extrapolated to zero GuHCl concentration (see Materials and Methods), is 23 kJ/mol of monomer (Table 1).

GuHCl-Induced Denaturation of Dfx Monitored by Far-UV CD. Native dfx shows a far-UV CD spectrum with a positive peak at 230 nm (most likely due to tyrosines, but

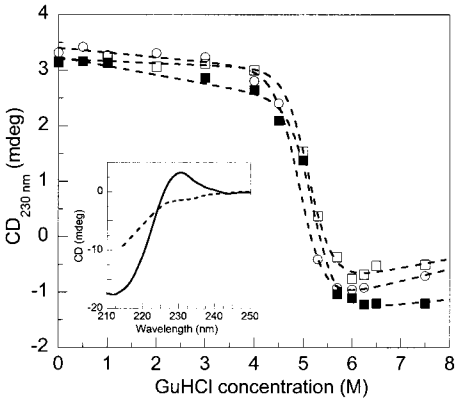

FIGURE 4: GuHCl-induced transitions in far-UV CD signals for various total dfx concentrations [(■) 1, (○) 5, and (□) 20 μM]. The inset shows the far-UV CD spectra of native/intermediate (—) and unfolded (- - -) dfx.

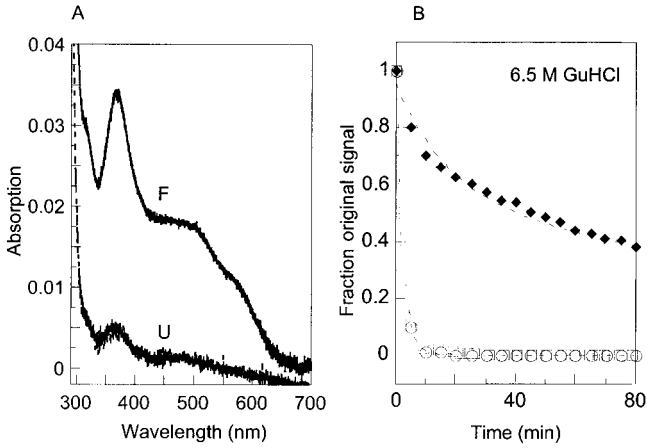

FIGURE 5: Optical absorption of ligand-to-metal charge transfer transitions in semireduced native (F) and unfolded (U) dfx. Time-resolved relative changes in far-UV CD (□), fluorescence (○), and absorption at 370 nm (◆) upon placing 5 μM dfx in 6.5 M GuHCl.

tryptophans may also contribute) and a negative peak at about 210 nm (due to the β-sheet structure). The far-UV CD spectra are similar for dfx at concentrations above and below the K_D (and the signal intensity varies linearly with dfx concentration), indicating that monomeric dfx can retain native-like structure. Upon addition of a high concentration of GuHCl to dfx, the intensities of the 230 and 210 nm signals decrease so that the overall far-UV CD spectrum changes toward one characteristic of a random coil polypeptide (Figure 4, inset). GuHCl-induced denaturation monitored by far-UV CD (at either 215 or 230 nm; the 230 nm data used for analyses due to less denaturant contribution) of dfx samples with different protein concentrations shows that the transition midpoints are independent of protein concentration in the 1−20 μM range (Figure 4). The dfx structure disappears with a transition midpoint around 5.1 M GuHCl in all cases (Table 1). Thus, by far-UV CD, a conformational change in dfx is monitored that agrees with a monomer to monomer transition. The average free energy in water for the disappearance of secondary structure, analyzed according to a two-state model (see Materials and Methods), is 49.5 kJ/mol of monomer (Table 1).

GuHCl-Induced Denaturation of Dfx Monitored by Visible Absorption. There are two iron centers in each dfx monomer (Figure 1) of which center I, Fe−$(S\text{-}Cys)_4$, is oxidized in the semireduced form, used in this study. Ligand-to-metal charge transfer in center I gives rise to absorption bands at 367 and 502 nm and shoulders at 317 and 567 nm (oxidation of the iron in center II yields additional absorption bands at 635 and 335 nm) (*24*). Upon addition of high concentrations of GuHCl to dfx, in combination with sufficiently long incubation times (5 h at 6 M GuHCl), the charge transfer transition disappears (Figure 5A). The equilibrium titration curve for this bleaching process shows a midpoint at 5.0 M GuHCl (data not shown). Thus, this transition takes place in parallel with far-UV CD disappearance ($[GuHCl]_{1/2} = 5.1$ M; Table 1) so that iron center I (probed by charge transfer absorption) remains intact as long as the secondary structure (monitored by far-UV CD) continues to be native-like. The fluorescence-detected equilibrium process (involving a change in dfx oligomeric state), however, does not perturb the environment of the iron in center I.

To further investigate the relation between dfx structure disappearance and iron charge transfer bleaching, we compared the unfolding kinetics (manual mixing) as monitored by changes in far-UV CD, fluorescence, and visible absorption upon placing 5 μM dfx in 6.5 M GuHCl (Figure 5B). Both the emission and CD changes occurred mostly within the mixing time (1 min) and are completed within 10−15 min (stopped-flow experiments are planned to determine actual rate constants), whereas the absorption bands disappeared much slower (Figure 5B). Two to three hours were required for complete bleaching of the charge transfer absorption under these conditions (5 μM dfx, 6.5 M GuHCl, pH 7). The kinetic results suggest that upon dfx polypeptide unfolding, iron center I remains intact initially, but slowly disassembles in the denatured state of the protein. The fact that the observed decrease in the level of charge transfer absorption corresponds to metal dissociation was first verified by the reactivity of cysteine sulfurs to Ellman's reagent in such samples. There are no other cysteines in dfx except the five involved in iron coordination, four in center I and one in center II (*23*). In accord, no free sulfurs were detected in dfx by the Ellman's reagent in the folded state. Up to 4 M GuHCl could be added to dfx without any observation of free sulfurs upon addition of Ellman's reagent. In 6 M GuHCl and after incubation for 5 h, however, free sulfurs in dfx were detected by the DTNB reaction (data not shown), in agreement with iron release (and, therefore, exposure of sulfurs) under these conditions. In another study, using only the N-terminal domain of dfx (and thus including only center I), iron dissociation (as a function of pH) was also monitored by a decrease in optical absorption (*32*). It was found in that system that iron reduction and cysteine oxidation occurred after metal dissociation from the polypeptide (*32*).

We also used the fluorescent indicator for iron Phen Green to probe iron dissociation under denaturing conditions. The emission of this phenanthroline−fluorescein dye at 520 nm (excitation at 492 nm) is strongly quenched upon iron binding (*33*). The emission from Phen Green in the presence of 5 μM dfx at various solution conditions was monitored (data not shown). The observed emission changes indicated iron release from dfx in 6 M GuHCl after incubation for 2 h (in accord with absorption and Ellman data). On the basis of an Fe(III) reference titration and the fact that there is more efficient Phen Green quenching by Fe(II) than by Fe(III) (see Materials and Methods), the observed quenching in the

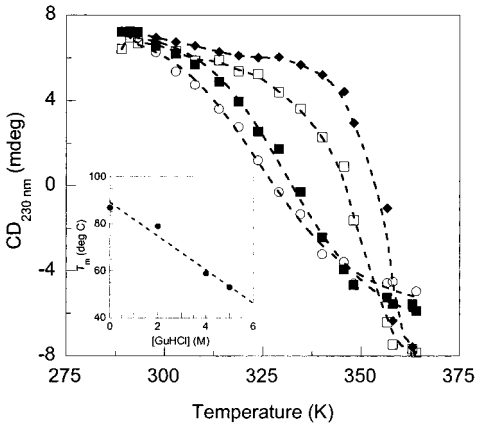

FIGURE 6: Thermal denaturation, as monitored by far-UV CD, of 2 μM dfx in the presence of various GuHCl concentrations [(◆) 0, (□) 2, (■) 4, and (○) 5 M GuHCl]. The inset shows T_m (kelvin) as a function of GuHCl concentration [T_m = 352 (2 M GuHCl), 330 (4 M GuHCl), 326 (5 M GuHCl), and ~360 K (0 M GuHCl)]. Linear extrapolation yields a T_m of 90 ± 3 °C (363 K) for 2 μM dfx in buffer.

presence of dfx in 6 M GuHCl corresponds roughly to dissociation of both irons (i.e., both center I and center II).

Reversibility of Dfx Denaturation. Dfx can refold into the native structure, as determined by emission maximum placement and the far-UV CD signal, after incubation at high GuHCl concentrations for up to 1 h (data not shown). The transition monitored by emission maxima is reversible also for longer incubation times (up to 5 h), if the protein is incubated in ≤5 M GuHCl. However, if the incubation time at ≥6 M GuHCl is increased to >1 h so that the ligand-to-metal charge transfer bands start to disappear (and iron dissociation is observed by Phen Green emission quenching), protein refolding is not possible. Only if the iron atoms (at least center I) do not dissociate from the unfolded polypeptide can dfx retain its native structure.

Thermally Induced Denaturation of Dfx. Denaturation of dfx was also induced by increased temperature and monitored by CD (200−260 nm). The thermal reaction was irreversible since there was no return of the characteristic CD signal or charge transfer absorption bands of native dfx upon cooling. Nevertheless, dfx appears to have high thermal stability. The thermal midpoint for 2 μM dfx is >80 °C, but a sufficient unfolded baseline could not be collected [Figure 6 (◆)]. To obtain an estimate of T_m for 2 μM dfx, we performed thermal experiments on dfx in the presence of 2, 4, and 5 M GuHCl (Figure 6) since additions of denaturant lower the transitions. Linear extrapolation in the plot of T_m versus denaturant concentration indicates a T_m of 90 ± 2 °C for 2 μM dfx in buffer (Figure 6, inset). The thermal transitions were irreversible, and therefore, no attempts to estimate thermodynamic parameters were performed.

Thermal melting monitored by far-UV CD appears to be protein concentration-dependent; 0.2 μM dfx (mostly monomeric species) displays a T_m of 79 ± 2 °C, whereas 20 μM dfx showed no unfolding up to 90 °C.

DISCUSSION

Since many proteins in the cell have multiple subunits as well as multiple domains and, in addition, coordinate a range of cofactors, studies of small, single-domain proteins with two-state transitions are not sufficient to explain the folding of all proteins. We have used the protein desulfoferrodoxin (dfx) as a model of a multidomain, oligomeric cofactor-binding protein (*23*−*25*) because it is a dimer of two monomers; each monomer has two domains and two iron cofactors. Despite this complexity, each dfx monomer contains no more than 128 residues and has a molecular mass of 14 kDa, which is within the normal range for monomeric proteins. The metal−$(S\text{-}Cys)_4$ motif, present in dfx center I as Fe−$(S\text{-}Cys)_4$, is one of the most common metal-binding motifs in biological systems (*32*). To elucidate the unfolding mechanism for the dfx dimer, and possible factors contributing to dfx's thermodynamic stability, we have used spectroscopic methods to probe dfx denaturation when induced by the chemical denaturant GuHCl as well as by heat.

Unfolding Mechanism of Dfx. We first established the dissociation constant for the dfx dimer (Figure 1). This result confirms the previous suggestion of dfx as a functional dimer (*29*, *30*), as well as gives a handle for estimating the ratio of dimer to monomer amounts at various studied protein concentrations. Equilibrium unfolding reactions induced by GuHCl additions, at different dfx concentrations, were monitored by tryptophan emission and far-UV CD (Figures 3 and 4). Strikingly different behavior is observed with the two methods. The shift in tryptophan emission maximum upon GuHCl additions is protein concentration-dependent, suggesting that this transition involves a dimer−monomer equilibrium. However, it is not solely dimer dissociation that is monitored since the emission change is in both its intensity and wavelength maximum. Upon dimer dissociation under native conditions, only a decrease in emission intensity is detected. Thus, the fluorescence-detected transition that takes place upon GuHCl addition appears to be that of dimer dissociation accompanied by some additional change that increases the level of exposure of the aromatic residues to the solvent. Since each dfx monomer is arranged in two domains, increased flexibility of these domains relative to each other may occur upon monomer−monomer dissociation in the presence of denaturant. In accord, the three tryptophans (contributing most of the emission) are located in domain II (W75, W87, and W121) near the domain−domain interface (highlighted in Figure 1). In support of a native-like structure of the monomeric dfx intermediate is the finding of no enhanced fluorescence from ANS in the presence of dfx in 2−4 M GuHCl (data not shown), as compared to ANS fluorescence in the presence of native or fully unfolded dfx. ANS is known to interact favorably with exposed hydrophobic surfaces (thereby increasing its emission); it is often used as a probe for intermediate structures of proteins. Furthermore, the fluorescence changes occur at 2−3 M GuHCl (Table 1) which are solution conditions under which no alteration of dfx's secondary structure is observed by far-UV CD (200−230 nm). Dfx's secondary structure does not disappear until 6 M GuHCl is added (the midpoint for the apparent two-state transition monitored by far-UV CD is 5.1 M GuHCl). We find no protein concentration dependence for the CD-monitored transition, in accord with dfx−dimer dissociation taking place at lower GuHCl concentrations in the fluorescence-monitored reaction.

Both fluorescence and far-UV CD transitions are fully reversible, as long as the incubation time in the denatured state is not too long at a denaturant concentration that is too high. By monitoring the absorption bands from the sulfur-

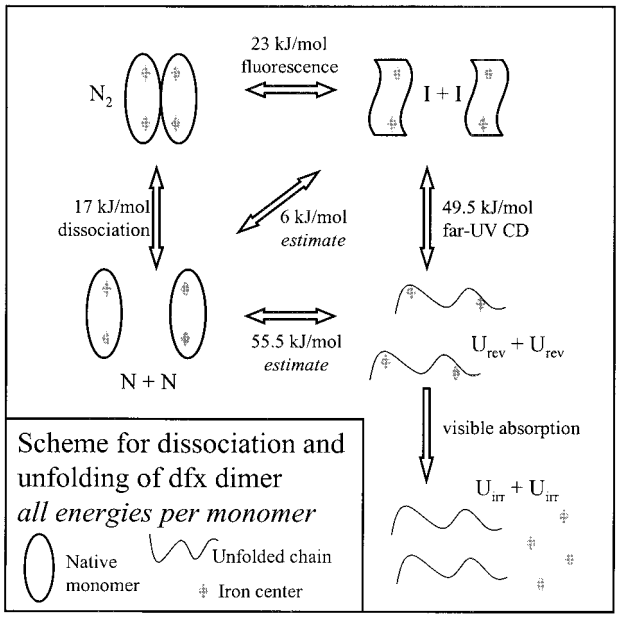

FIGURE 7: Tentative scheme for the interplay of dfx folding−unfolding and assembly−disassembly processes (see the text for a discussion).

to-iron charge transfer transition of center I, we could probe changes in the coordination sphere of the oxidized iron in domain I. The charge transfer bands bleach in a transition identical to that monitored by far-UV CD. However, for each dfx sample to reach its equilibrium absorption value in or after the transition region, an incubation time longer than that used to obtain equilibrium CD signals at each point was required. This difference was clearly shown in the time-resolved unfolding experiment presented in Figure 5B, in which spectroscopic changes upon placing dfx in a high GuHCl concentration are compared in real time. Both emission and CD changes equilibrate quickly, whereas optical absorption decreases over a longer time span. Thus, dfx first dissociates into monomers, and the polypeptide unfolds (as monitored by emission and far-UV CD). Not until after unfolding do the iron atoms slowly dissociate (as monitored by visible absorption and the iron indicator Phen Green). This conclusion is in accord with the refolding results. If enough time is allowed in the denatured state, at high GuHCl concentrations favoring polypeptide unfolding, the irons dissociate and refolding is not possible. On the other hand, if the incubation time in the denatured state is shorter, so that metal dissociation is minimal, native dfx can be retained.

In Figure 7, we present a scheme that explains our experimental data on the dfx denaturation process. The dimer first dissociates, at low denaturant concentrations, to monomers with native-like secondary structure but with tryptophan emission like the unfolded state ($N_2 \Leftrightarrow 2I$). The free energy associated with this conformational change in each monomer, yielding solvent exposure of aromatic residues, was estimated from the difference in dissociation free energy (not including a structural change, 17 kJ/mol of monomer) and the energy of the fluorescence-detected transition (dissociation and structural change, 23 kJ/mol of monomer) to be around 6 kJ/mol of monomer. This is a rather low value, in accord with a minor change (such as increased flexibility of, or solvent insertion in, the domain−domain interface in each monomer) not resolved by far-UV CD. The dfx monomers are significantly resistant to the denaturant, and not until 5 M GuHCl is added does the secondary structure start to disappear in a transition corresponding to a free energy change of 49.5 kJ/mol of monomer ($I \Leftrightarrow U_{rev}$). The unfolded protein initially retains iron center I; however, over time the iron in center I disassembles from the polypeptide, creating an irreversibly denatured state ($U_{rev} \Rightarrow U_{irr}$ + iron). It is likely that the iron in center II follows the same path, but there is no direct evidence yet (albeit the Phen Green experiments strongly support this). We used the data in Figure 7 to estimate the free energy change associated with the transition from one native dimer to two unfolded monomers retaining the irons ($N_2 \Leftrightarrow 2U_{rev}$) to be about 145 kJ/mol of dimer.

Dfx Unfolding Compared to That of Other Oligomeric Proteins. The free energy estimated for dfx dimer stability, 145 kJ/mol of dimer, is large for a protein this size (28 kDa). For comparison, the stability of the SecA dimer (molecular mass of 102 kDa) was found to be 94 kJ/mol of dimer (*6*). Also, other dimeric proteins such as *E. coli* Trp repressor, creatine kinase bacterial luciferase, and glutathione transferases exhibit folding free energies in the range of 80−125 kJ/mol of dimer (*34*−*36*). The stability of the average dimeric protein seems to be higher than that of the average monomeric protein (normal range is 20−40 kJ/mol of monomer), indicating that subunit−subunit interaction can increase the stability of a protein (*6*). In the case of the dfx dimer, we estimate that around 77% [(55.5 kJ/mol of monomer)/(17 + 55.5 kJ/mol of monomer)] of the free energy originates within the structure of each monomer and only 23% is due to subunit−subunit interactions. During dfx unfolding, the dimer *first* dissociates into monomeric structures, in accord with the interface interactions being weaker than those within the monomers; not until higher denaturant concentrations are added do the monomers unfold. It is possible that the polar nature of the dfx monomer−monomer interface, which is a rather unusual feature of a protein interface, helps promote dissociation prior to polypeptide unfolding. In the dfx crystal structure (*29*), the monomer−monomer interface was found to consist of an open polar core, including a calcium ion and six water molecules, with regions below and above containing a high density of aromatic residues (Figure 1).

In Table 2, we have summarized available thermodynamic data for a number of oligomeric proteins. The proteins are divided into three groups according to the proposed unfolding mechanisms. It appears as if large (α-helical) oligomeric proteins (molecular mass > 35 kDa per monomer) unfold through oligomeric intermediates. If the monomer is small in size (molecular mass < 20 kDa per monomer), the equilibrium unfolding mechanism is instead likely to be an apparent two-state process. If the monomer unit has an intermediate size (20−30 kDa), or if it is small but has a high stability per monomer (like dfx and GroES; 72 and 38 kJ/mol of monomer, respectively), unfolding may proceed through folded or intermediate state monomers (Table 2). Notably, peanut agglutinin (*1*), which like dfx has an open oligomeric structure with rather weak interface interactions, also unfolds through a folded monomeric species. Oligomeric proteins often bury a larger fraction of nonpolar surface than most globular (monomeric) proteins. For monomeric proteins, the change in total accessible surface area upon unfolding is linearly dependent on both the number of

Table 2: Thermodynamic Parameters for Equilibrium Unfolding of Oligomeric Proteins[a]

protein	no. of subunits	secondary structure	molecular mass (kDa/ monomer)	ΔG_u (kJ/mol of oligomer)	ref
$F_{oligo} \rightarrow I_{oligo}$ or $U_{oligo} \rightarrow U_{mon}$ (i.e., oligomeric intermediate)					
lactose repressor	4	α	38	250	*4*
SecA	2	α	102	95	*6*
GroEL	14	α	57	nd	*40*
$F_{oligo} \rightarrow F_{mon}$ or $I_{mon} \rightarrow U_{mon}$ (i.e., monomeric intermediate)					
peanut agglutinin	4	*β*	27	37	*1*
glutathione transferase	2	α+*β*	25	∼100	*5*
GroES	7	*β*	10	264	*31*
Dfx	2	*β*	14	145	−
$F_{oligo} \rightarrow U_{mon}$ (i.e., apparent two-state process)					
SecB	4	α+*β*	17	118	*3*
Cpn10	7	*β*	10	216	*7*
archaeal histones	2	α+*β*	8	60	*41*
Arc repressor	2	α+*β*	7	40	*42*
E2 DNA-binding domain	2	*β*	9	nd	*43*
C_H3 domain	2	*β*	12	66	*44*

[a] The proteins are divided into three groups according to their proposed equilibrium unfolding mechanisms. nd, not determined.

residues in the protein and the change in heat capacity upon unfolding (*3*). Oligomeric proteins, however, tend to have lower than expected changes in heat capacity upon unfolding; this was suggested to be due to incomplete unfolding in some cases (*3*). In addition, it was found that a large oligomeric protein buries a larger fraction of its total surface area than a smaller oligomeric protein (*3*). Since there are relatively few studies reported on thermal unfolding of multimeric proteins, because of their tendency to undergo irreversible denaturation (as is also the case for the thermal unfolding of dfx reported here), general conclusions are difficult to make.

Dfx Structure Is Unusually Stable. The monomeric protein onconase, a member of the RNAse superfamily which is only 104 residues long with two *β*-sheets and three helices, was reported to have an unusually high thermodynamic stability of almost 60 kJ/mol of monomer (*37*). A combination of protein compactness, short loops, and a disulfide bridge toward the C-terminus was put forward as a possible explanation. Using the scheme in Figure 7, we estimated unfolding of one dfx monomer (128 residues) to correspond to a free energy change of 55.5 ± 2 kJ/mol of monomer, which is on the same order of magnitude as that determined for onconase. The monomeric structure of dfx thus appears to have an intrinsically high stability, which is only somewhat increased by the monomer−monomer interactions. This high stability is most likely due to the iron centers holding the polypeptide in place. It should be mentioned here that none of the other oligomeric proteins listed in Table 2 (except SecA that is suggested to have a zinc-binding site) coordinate metals. Support for the importance of the irons in determining the dfx stability comes from the finding that iron center I remains intact after polypeptide unfolding; only slowly do the metals dissociate from the polypeptide in the denatured state. It has been reported for at least two other iron proteins, HiPIP from *C. vinosum* and a thermophilic ferredoxin, that the iron−sulfur clusters are important for stability and that they can remain coordinated also when the polypeptides have unfolded (*20*, *21*). The fact that the $Fe-(S\text{-}Cys)_4$ center in domain I of dfx is strongly bound to the native polypeptide was shown by pH titration; this center remained stable in the protein scaffold down to pH 2.0 (*32*).

A recent report in the literature compared sequences of putative soluble proteins from the complete genomes of eight thermophiles and twelve mesophiles to gain insight into determinants of protein thermostability (*38*). With respect to amino acid composition, significant increases in the relative amount of charged (Arg, Lys, and Glu) and hydrophobic (Val, Ile, Gly, and Pro) amino acids and decreases in the relative amount of uncharged polar amino acids (Gln, Asn, and Thr) in proteins from thermophiles, relative to mesophilic organisms, were reported. We find that the distribution of residues in the dfx primary structure follows a pattern more similar to that of the thermophiles than to that of the mesophilic proteins. Dfx has significantly large amounts of Glu and Lys as well as of Val, Pro, and Gly residues, whereas the number of Gln and the number of Asn amino acids are low. Since Asn and Gln deamination occurs readily in peptides at high temperatures, a low content of Gln and Asn residues in dfx (and in thermophilic proteins in general) could increase chemical stability at higher temperatures (*39*). Many factors are, however, involved in governing protein thermostability, and dfx is not as thermodynamically stable as proteins isolated from thermophiles. Thermostable iron-binding monomeric proteins have been shown to display T_m's in the range of 120−200 °C and folding free energies (at 20 °C) most often higher than 60 kJ/mol (*21*).

ACKNOWLEDGMENT

We thank Prof. J. LeGall and Dr. Y. Liu (University of Georgia, Athens, GA) for providing protein and Dr. N. Horton (University of California, Santa Barbara, CA) for help with Figure 1.

REFERENCES

1. Reddy, G. B., Bharadwaj, S., and Surolia, A. (1999) *Biochemistry 38*, 4464−70.
2. Dams, T., and Jaenicke, R. (1999) *Biochemistry 38*, 9169−78.
3. Panse, V. G., Swaminathan, C. P., Aloor, J. J., Surolia, A., and Varadarajan, R. (2000) *Biochemistry 39*, 2362−9.
4. Barry, J. K., and Matthews, K. S. (1999) *Biochemistry 38*, 6520−8.
5. Hornby, J. A., Luo, J. K., Stevens, J. M., Wallace, L. A., Kaplan, W., Armstrong, R. N., and Dirr, H. W. (2000) *Biochemistry 39*, 12336−44.
6. Doyle, S. M., Braswell, E. H., and Teschke, C. M. (2000) *Biochemistry 39*, 11667−76.
7. Guidry, J., Moczygemba, C., Steede, K., Landry, S., and Wittung-Stafshede, P. (2000) *Protein Sci. 9*, 2109−17.
8. Robinson, C. R., Liu, Y., Thomson, J. A., Sturtevant, J. M., and Sligar, S. G. (1997) *Biochemistry 36*, 16141−6.
9. Leckner, J., Bonander, N., Wittung-Stafshede, P., Malmstrom, B. G., and Karlsson, B. G. (1997) *Biochim. Biophys. Acta 1342*, 19−27.
10. Hargrove, M. S., and Olson, J. S. (1996) *Biochemistry 35*, 11310−8.
11. Falzone, C. J., Mayer, M. R., Whiteman, E. L., Moore, C. D., and Lecomte, J. T. (1996) *Biochemistry 35*, 6519−26.
12. Wittung-Stafshede, P., Lee, J. C., Winkler, J. R., and Gray, H. B. (1999) *Proc. Natl. Acad. Sci. U.S.A. 96*, 6587−90.
13. Apiyo, D., Guidry, J., and Wittung-Stafshede, P. (2000) *Biochim. Biophys. Acta 1479*, 214−24.

14. Luisi, D. L., Wu, W. J., and Raleigh, D. P. (1999) *J. Mol. Biol. 287*, 395−407.
15. Shortle, D. R. (1996) *Curr. Opin. Struct. Biol. 6*, 24−30.
16. Wittung-Stafshede, P., Gomez, E., Ohman, A., Aasa, R., Villahermosa, R. M., Leckner, J., Karlsson, B. G., Sanders, D., Fee, J. A., Winkler, J. R., Malmstrom, B. G., Gray, H. B., and Hill, M. G. (1998) *Biochim. Biophys. Acta 1388*, 437−43.
17. Wittung-Stafshede, P., Malmstrom, B. G., Winkler, J. R., and Gray, H. B. (1998) *J. Phys. Chem. 102*, 5599−601.
18. Wittung-Stafshede, P., Hill, M. G., Gomez, E., Di Bilio, A., Karlsson, G., Leckner, J., Winkler, J. R., Gray, H. B., and Malmstrom, B. G. (1998) *J. Biol. Inorg. Chem. 3*, 367−70.
19. Wittung-Stafshede, P., Malmstrom, B. G., Sanders, D., Fee, J. A., Winkler, J. R., and Gray, H. B. (1998) *Biochemistry 37*, 3172−7.
20. Bertini, I., Cowan, J. A., Luchinat, C., Natarajan, K., and Piccioli, M. (1997) *Biochemistry 36*, 9332−9.
21. Wittung-Stafshede, P., Gomes, C. M., and Teixeira, M. (2000) *J. Inorg. Biochem. 78*, 35−41.
22. Wittung-Stafshede, P. (1998) *Biochim. Biophys. Acta 1382*, 324−32.
23. Devreese, B., Tavares, P., Lampreia, J., Van Damme, N., Le Gall, J., Moura, J. J., Van Beeumen, J., and Moura, I. (1996) *FEBS Lett. 385*, 138−42.
24. Tavares, P., Ravi, N., Moura, J. J., LeGall, J., Huang, Y. H., Crouse, B. R., Johnson, M. K., Huynh, B. H., and Moura, I. (1994) *J. Biol. Chem. 269*, 10504−10.
25. Moura, I., Tavares, P., Moura, J. J., Ravi, N., Huynh, B. H., Liu, M. Y., and LeGall, J. (1990) *J. Biol. Chem. 265*, 21596−602.
26. Pianzzola, M. J., Soubes, M., and Touati, D. (1996) *J. Bacteriol. 178*, 6736−42.
27. Smith, D. R., Doucette-Stamm, L. A., Deloughery, C., Lee, H., Dubois, J., Aldredge, T., Bashirzadeh, R., Blakely, D., Cook, R., Gilbert, K., Harrison, D., Hoang, L., Keagle, P., Lumm, W., Pothier, B., Qiu, D., Spadafora, R., Vicaire, R., Wang, Y., Wierzbowski, J., Gibson, R., Jiwani, N., Caruso, A., Bush, D., Reeve, J. N., et al. (1997) *J. Bacteriol. 179*, 7135−55.
28. Fraser, C. M., Norris, S. J., Weinstock, G. M., White, O., Sutton, G. G., Dodson, R., Gwinn, M., Hickey, E. K., Clayton, R., Ketchum, K. A., Sodergren, E., Hardham, J. M., McLeod, M. P., Salzberg, S., Peterson, J., Khalak, H., Richardson, D., Howell, J. K., Chidambaram, M., Utterback, T., McDonald, L., Artiach, P., Bowman, C., Cotton, M. D., Venter, J. C., et al. (1998) *Science 281*, 375−88.
29. Coelho, A., Matias, P., Fulop, V., Thompson, A., Gonzalez, A., and Carrondo, M. (1997) *J. Biol. Inorg. Chem. 2*, 680−9.
30. Verhagen, M. F., Voorhorst, W. G., Kolkman, J. A., Wolbert, R. B., and Hagen, W. R. (1993) *FEBS Lett. 336*, 13−8.
31. Higurashi, T., Nosaka, K., Mizobata, T., Nagai, J., and Kawata, Y. (1999) *J. Mol. Biol. 291*, 703−13.
32. Kennedy, M., Yu, L., Lima, M. J., Ascenso, C., Czaja, C., Moura, I., Moura, J., and Rusnak, F. (1998) *J. Biol. Inorg. Chem. 3*, 643−9.
33. Petrat, F., de Groot, H., and Rauen, U. (2000) *Arch. Biochem. Biophys. 376*, 74−81.
34. Gloss, L. M., and Matthews, C. R. (1997) *Biochemistry 36*, 5612−23.
35. Clark, A. C., Sinclair, J. F., and Baldwin, T. O. (1993) *J. Biol. Chem. 268*, 10773−9.
36. Fan, Y. X., Zhou, J. M., Kihara, H., and Tsou, C. L. (1998) *Protein Sci. 7*, 2631−41.
37. Notomista, E., Catanzano, F., Graziano, G., Dal Piaz, F., Barone, G., D'Alessio, G., and Di Donato, A. (2000) *Biochemistry 39*, 8711−8.
38. Chakravarty, S., and Varadarajan, R. (2000) *FEBS Lett. 470*, 65−9.
39. Michelitsch, M. D., and Weissman, J. S. (2000) *Proc. Natl. Acad. Sci. U.S.A. 97*, 11910−5.
40. Chen, J., and Smith, D. L. (2000) *Biochemistry 39*, 4250−8.
41. Li, W. T., Grayling, R. A., Sandman, K., Edmondson, S., Shriver, J. W., and Reeve, J. N. (1998) *Biochemistry 37*, 10563−72.
42. Bowie, J. U., and Sauer, R. T. (1989) *Biochemistry 28*, 7139−43.
43. Mok, Y. K., Alonso, L. G., Lima, L. M., Bycroft, M., and de Prat-Gay, G. (2000) *Protein Sci. 9*, 799−811.
44. Thies, M. J., Mayer, J., Augustine, J. G., Frederick, C. A., Lilie, H., and Buchner, J. (1999) *J. Mol. Biol. 293*, 67−79.

BI002653Y